Mass Spectrometry
DOI: 10.5702/massspectrometry.A0071

Vol. 7 (2018), A0071

Original Article

Generation and Propagation of MALDI Ion Packets Probed by Sheet-Like Nanosecond UV Laser Light

Tatsuro Shirota and Kennosuke Hoshina*

Faculty of Pharmaceutical Sciences, Niigata University of Pharmacy and Applied Life Sciences, 265–1 Higashijima, Akiha-ku, Niigata 956–8603, Japan

A sheet-like ultraviolet (UV) probe laser is used to investigate the ejection and propagation of ion packets of matrix CHCA, which are produced by matrix-assisted laser desorption and ionization (MALDI). Laser irradiation of the expanding MALDI plume induced photodissociation of the CHCA-related ions, which existed in a sheet-like volume, leading to their absence in their MALDI signal profiles. The MALDI spectra were measured under varying conditions: the temporal delay of the lasers and the distance of the sheet-like probe laser from the MALDI sample surface. It was found that the center of the $(CHCA)H^+$ packets were ejected at 46±11 ns after MALDI laser irradiation, while the $(CHCA)_2H^+$ packets were ejected at 64±12 ns, regardless of the magnitude of acceleration static high-voltage in 3.5–5.5 kV. This suggests that $(CHCA)_2H^+$ is formed by a proton transfer reaction from $(CHCA)H^+$ to $(CHCA)_2$ in the heated condensed phase and/or near the surface. This study represents the first experimental determination of ion ejection time in the MALDI process, which is also applicable to other species in the MALDI plume.

Please cite this article as: Mass Spectrom (Tokyo) 2018; 7(1): A0071

Keywords: MALDI, proton transfer, CHCA, photodissociation, Time-of-Flight (TOF) mass spectrometry

(Received April 23, 2018; Accepted November 9, 2018)

INTRODUCTION

Matrix-assisted laser desorption and ionization mass spectrometry (MALDI-MS) is widely used in biological sciences as a technique for ionizing and detecting nonvolatile high-mass biomolecules, such as peptides and proteins, with minimal fragmentation.[1–3] After the matrix and sample mixtures are irradiated by the laser, the resulting liquid phase or dense gas plume will produce analyte ions by proton transfer from the protonated matrix molecules to the intact analyte molecules.[4–9] However, the time scale of matrix and analyte ion formation processes have not been elucidated in the rapidly changing conditions that are inherent in the MALDI process, which includes ultraviolet (UV) laser absorption by matrix molecules and a rapid increase in temperature, followed by the melting and vaporization of polycrystals.[10–12] It was demonstrated that molecular ion ejection mainly occurs from fragment clusters which are formed just after expansion of the target crystal through laser heating rather than evaporation simply from the surface.[10,13–24]

According to a theoretical study, the interrelation between the physical and chemical processes in MALDI affects the signals and detection sensitivity.[25] However, the formation of protonated ions is likely to be completed within tens of nanoseconds near the laser-irradiated surface[25]; therefore, it is difficult to trace this quick chemical process in the MALDI plume which expands only to several tens of μm from the surface.[26,27] Even so, the expanded MALDI plume may exhibit the memory of every chemical reactions that do not necessarily proceed on the same timescale.[9,19,28–30] Spatiotemporal distribution that depends on chemical species must contain information to clue the chemical processes in a hot and dense MALDI plume expanding just after laser irradiation.

A few successful investigations of the physical and chemical processes in MALDI have been conducted by probing the plume. Puretzky *et al.* measured the spatiotemporal distribution of the expanding neutral species using laser-induced fluorescence imaging 10 μs after laser irradiation and estimated their initial velocity to be 500–1000 ms^{-1}.[28,29] Bökelmann *et al.* investigated the $(DHB)H^+$ distribution 1 μs after the laser irradiation of substance P and DHB mixture and concluded that proton transfer efficiently proceeds from $(DHB)H^+$ with low initial velocity to the analytes.[30] These previous studies have probed the propagation of MALDI plumes without an accelerating electric field in which more than several μs was required to propagate to a detectable region that resulted in a temporal resolution in the order of 1 μs. Therefore, the ion packet must be extracted and accelerated to trace the generation/ejection processes

*Correspondence to: Kennosuke Hoshina, *Faculty of Pharmaceutical Sciences, Niigata University of Pharmacy and Applied Life Sciences, 265–1 Higashijima, Akiha-ku, Niigata 956–8603, Japan*, e-mail: hoshina@nupals.ac.jp

of ionic species from the surface that was observed over a period of several tens of ns with a comparable temporal resolution.

In the present study, a method that uses a sheet-like probe UV laser is proposed to trace the propagation of ion packets that are ejected by the MALDI process. Based on the spatiotemporal position of the $(CHCA)H^+$ and $(CHCA)_2H^+$ ion packets, the time lag that was required to release the packets from the MALDI target surface after laser irradiation was also examined.

EXPERIMENTAL

Sample Preparation

α-Cyano-4-hydroxycinnamic acid (CHCA), acetonitrile with 0.1% trifluoroacetic acid (TFA), and ultrapure water that were purchased from Wako Pure Chemical Industries, Ltd. were used during the current study; CHCA was used without further purification. The MALDI samples were prepared using the dried droplet method[31] at room temperature under atmospheric pressure. Specifically, a 40-μL CHCA solution (50 μmol/mL in 1:1 solution of acetonitrile with 0.1% TFA and ultrapure water) was deposited on a stainless steel stage. The typical size of a dried sample, which contained only the matrix molecule of CHCA, exhibited a diameter of 5 mm.

Measurement

Figure 1 shows the experimental setup for this study. The MALDI samples were irradiated with the 3rd harmonic of Q-sw Nd:YAG laser light (LASER-1, 355 nm, 5 ns, 10 Hz, Quanta-Ray GCR-3; Spectra-Physics) at an incident angle of 30°, which induced the MALDI process. The laser spot size on the sample surface was estimated to be 1 mm in diameter, which indicated a laser fluence of 7.0–7.5 $mJcm^{-2}$ per pulse. The ions that were ejected through the MALDI process were typically accelerated at +4.5 kV (3.54×10^5 Vm^{-1}) and were detected by the microchannel plate through a linear-type time-of-flight (TOF) mass spectrometer (Jordan TOF Products, Inc.). The ion signals were further digitized (5 GS/s) on an oscilloscope, transferred to a PC, and averaged over approximately 20 shots.

Another 3rd harmonic of a YAG laser beam (LASER-2, 355 nm, 5 ns, 10 Hz, Quanta-Ray INDI; Spectra-Physics) that was cut out with a 1-mm slit, which generated sheet-shaped laser light (7 mm in length and 1 mm in height), was introduced into the MALDI plume that was generated by the MALDI laser irradiation, as shown in Fig. 1. The laser fluence at the irradiation spot was estimated to be 100–115 $mJcm^{-2}$ per pulse. The LASER-1 and LASER-2 pulses were synchronized with each other by a delay generator (DG645, Stanford research Co.) with a temporal jitter of 1 ns. When

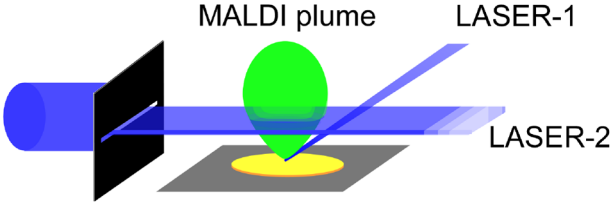

Fig. 1. Experimental scheme for probing the MALDI plume using a sheet-like UV laser.

the ions in the sheet-like volume that were irradiated by LASER-2 were dissociated into smaller fragment ions, a partial decrease in the number of the ions in the MALDI plume was expressed as a partial absence of its signal profile in the MALDI-MS spectrum. Because this information was obscured using a reflectron-type mass spectrometer, which can compensate for the spread of signal profile due to the initial velocity distribution, the linear-type spectrometer was chosen.

The MALDI-MS spectra can be measured as a function of Δt and z, where Δt is the temporal delay of LASER-2 from the time at which the temporal center of LASER-1 light pulses irradiate the sample surface and z is the distance of the sheet-like LASER-2 beam path with a thickness of 1 mm from the sample surface. The propagation of ion packets can be tracked by measuring (Δt, z) when the center of the MALDI signal is missing.

RESULTS AND DISCUSSION

Observed MALDI-TOF spectra

Figure 2a shows the MALDI-TOF spectrum of CHCA obtained by LASER-1 irradiation. The typical MALDI signals of $(CHCA\text{-}H_2O)H^+$ (m/z 172), $(CHCA)H^+$ (m/z 190), $(CHCA)_2H^+$ (m/z 379), and $(CHCA)Na^+$ (m/z 212) are detected. It is well known that the alkali metal adduct signals originate from the impurities in samples or instruments. Because a linear-type mass spectrometer was used, each peak exhibited a wide spectral width because of the initial velocity distribution. Figure 2b shows a MALDI-TOF spectrum that is obtained when LASER-2 is irradiated after LASER-1 at z=0.6–1.6 mm and a temporal delay of Δt=150 ns. z=0.6–1.6 mm indicates that the sheet-like laser with a thickness of 1 mm covers the region of z=0.6 to 1.6 mm. This was the closest position of LASER-2 at which measurements could be conducted without any MALDI signals from LASER-2.

There are two drastic differences in Fig. 2b relative to Fig. 2a, which include the appearance of small signals in the low-mass region and the partial absence of the CHCA-related ion peaks such as $(CHCA)H^+$. The appearance of small signals by LASER-2, which were assigned to the $C_nH_m^+$ series of fragment ions, and the partial absence in the CHCA-related peaks were observed in the same spectra throughout the present measurement. This suggests that a part of the ion packet existed in the region of z=0.6–1.6 mm and that it was reduced by photodissociation, leading to the absence of the $(CHCA)H^+$ signals and the appearance of the fragment ion signals. Based on the extent of parts that were missing in the peaks, the volume irradiated with a thickness of 1 mm by LASER-2 was observed to be approximately one-third of the full size of the ion packet that propagated in the z=0.6–1.6 mm region.

MALDI-TOF spectra measured by changing z and Δt

A series of MALDI-TOF spectra were measured by varying Δt from 0 to 500 ns with intervals of 50 ns at a fixed z value, and the comparison of the spectra is presented in Fig. 3. The arrows show the positions at which the missing ion signals are observed in $(CHCA)H^+$ by irradiation using LASER-2. At z=0.6–1.6 mm, the missing position began to appear on the left part of $(CHCA)H^+$

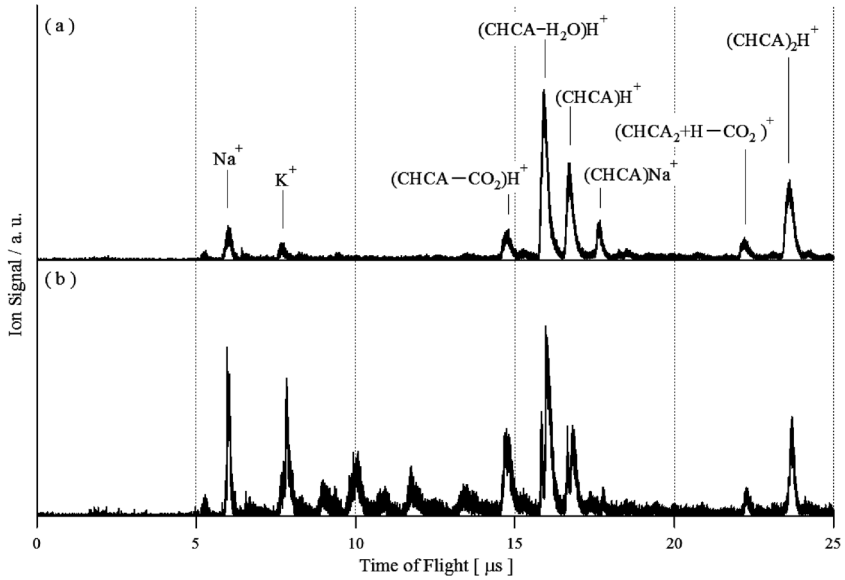

Fig. 2. (a) The MALDI-TOF spectra of CHCA without probe laser and (b) with probe laser irradiation (b) at Δt=100 ns and z=0.6–1.6 mm.

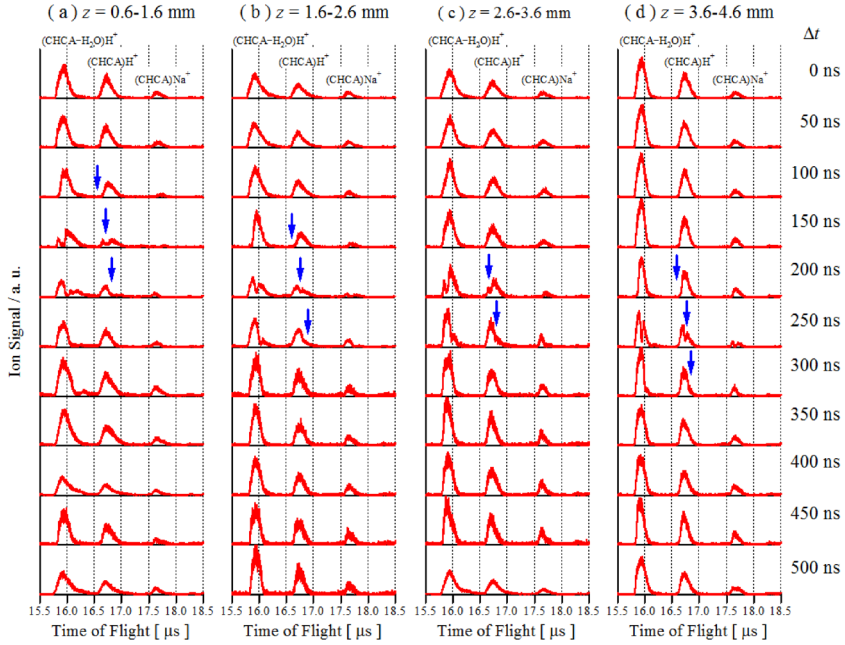

Fig. 3. The MALDI-TOF spectra in the region where $(CHCA)H^+$ signals are observed with the probe laser irradiation that is measured by varying Δt at a fixed z to (a) 0.6–1.6 mm, (b) 1.6–2.6 mm, (c) 2.6–3.6 mm, and (d) 3.6–4.6 mm.

peak at Δt=100 ns, which corresponded to the time at which the head of the ion packet was irradiated and at which the ions were dissociated by LASER-2. The missing position moves to the central part of the MALDI signal at Δt=150 ns and the right part at Δt=200 ns, corresponding to LASER-2 irradiation at the central and the back parts of the ion packet, respectively. This indicates that the packet passed through the region of z=0.6–1.6 mm within the interval of Δt=100–200 ns. The temporal delay of the observed partial signal shifts to longer Δt as z increases; Δt=100–200 ns at z=0.6–1.6 mm, Δt=150–250 ns at z=1.6–2.6 mm, Δt=200–250 ns at z=2.6–3.6 mm, and Δt=200–300 ns at z=3.6–4.6 mm. Because z corresponds to the propagation distance of the ion packet, it is reasonable to expect longer Δt for partial signals as z increases. Similar partial missing signals were observed in the $(CHCA\text{-}H_2O)H^+$ and $(CHCA)Na^+$ peaks. There are no new signals in the TOF spectra of (z, Δt)=(0.6–1.6, 500) with the second laser irradiation. In addition, fragment ions seen in the lower mass region appear only when ion missing are observed in the profiles of $(CHCA)H^+$, $(CHCA)_2H^+$. This indicates that post-ionization of neutral species does not occur in the present observation.

Figure 4 shows the TOF region of $(CHCA)_2H^+$. In addition, the missing signals can be labeled using arrows. The partial missing signals were observed at Δt=100–300 ns when z=0.6–1.6 mm, Δt=200–350 ns when z=1.6–2.6 mm, Δt=250–400 ns when z=2.6–3.6 mm, and Δt=250–450 ns when z=3.6–4.6 mm. The partial missing signal of $(CHCA)_2H^+$ exhibited a longer Δt than that exhibited by $(CHCA)H^+$, indicating that the propagation velocity of the former was smaller. It is because of its higher mass,

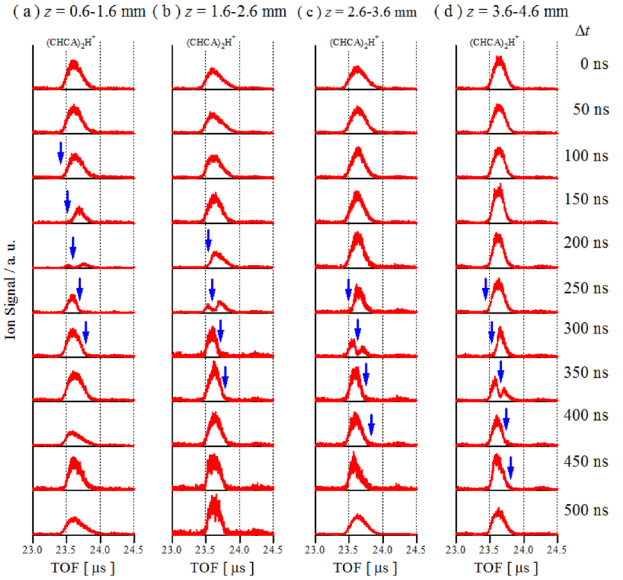

Fig. 4. The MALDI-TOF spectra in the region where $(CHCA)_2H^+$ signals are observed with the probe laser irradiation that is measured by changing Δt at a fixed z to (a) 0.6–1.6 mm, (b) 1.6–2.6 mm, (c) 2.6–3.6 mm, and (d) 3.6–4.6 mm.

which was approximately double that of the latter.

Propagation of ion packets

The missing of the profile center at (z, Δt) indicates that the center of the ion packet passes position z at time Δt. Therefore, we surveyed the condition (Δt, z) at which the center of the $(CHCA)H^+$ profile was observed to decrease by changing z at a 1-mm step. Figures 5(a) and (b) plot (Δt, z) for $(CHCA)H^+$ and $(CHCA)_2H^+$, corresponding to the propagated distance of the ion packet center, which was obtained for the three acceleration voltages of +3.5 kV (2.76×10^5 Vm^{-1}), +4.5 kV (3.54×10^5 Vm^{-1}), and +5.5 kV (4.33×10^5 Vm^{-1}). Although Δt was measured at a fixed z, a minor correction was made to z by considering the ratio of the resultant forward and backward peaks that remained after LASER-2 irradiation.

As expected, $(CHCA)H^+$ propagated faster than $(CHCA)_2H^+$; further, the propagation rate increased as the acceleration voltage increased. In classical mechanical treatment, the propagated distance, z, is expressed by

$$z = v_0(\Delta t - t_E) + \frac{eE}{2m}(\Delta t - t_E)^2, \quad (1)$$

where t_E is the time required for free molecule ion ejection from surface and/or clusters with mass, m, and an initial velocity, v_0, after irradiation by LASER-1, E is the electric field for acceleration, and e is the elementary charge. As shown by the solid lines in Fig. 5(a), the observed (Δt, z) plot of $(CHCA)H^+$ is reproduced by Eq. (1) when t_E is set at 45 ns. The ejection velocity, v_0, was assumed to be 500 ms^{-1}, which was obtained from previous reports[15,32] although it has been demonstrated that the velocities span a very wide range,[33] v_0 was observed to minorly affect propagation because the first term in Eq. (1) was considerably smaller than the second term. Similarly, $(CHCA)_2H^+$ data was reproduced when t_E=65 ns, which was 20 ns behind the ejection of $(CHCA)H^+$.

Figure 6 shows histograms of the t_E values determined

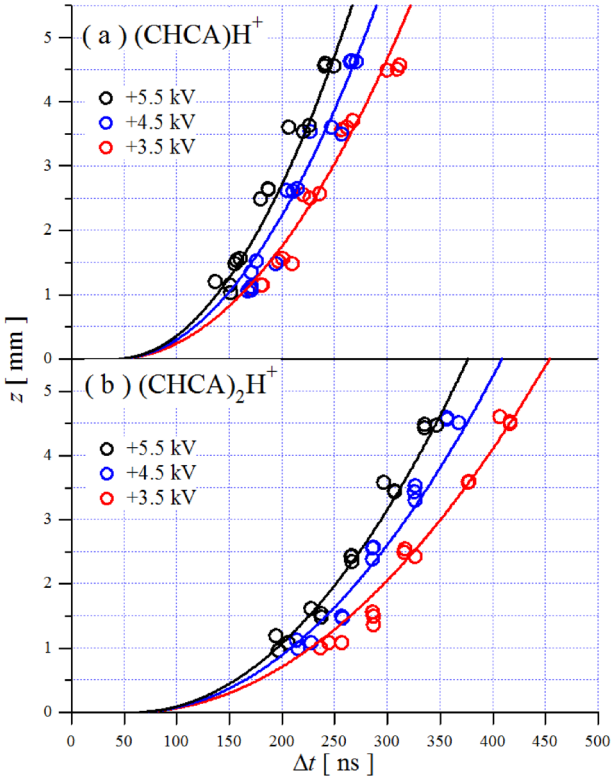

Fig. 5. Plots of (Δt, z) at which missing signals were observed in the center of the MALDI profiles for (a) $(CHCA)H^+$ and (b) $(CHCA)_2H^+$ at three acceleration voltages, +3.5, +4.5, and +5.5 kV. The solid lines are the simulations of ion propagation when t_E is set to be 45 ns for $(CHCA)H^+$ and 65 ns for $(CHCA)_2H^+$.

for each (Δt, z) point in Fig. 5. Although the distribution of t_E exhibited widths as large as 30–35 ns, the difference in t_E between $(CHCA)H^+$ and $(CHCA)_2H^+$ was significant; t_E of $(CHCA)H^+$ was smaller than that of $(CHCA)_2H^+$. The average values of t_E for $(CHCA)H^+$ at three acceleration voltages were 48±10, 49±11, and 40±8 ns at +3.5, +4.5, and +5.5 kV, respectively, whereas those of $(CHCA)_2H^+$ were 70±13, 62±13, and 62±8 ns. The overall average values of t_E were 46±11 and 64±12 ns for $(CHCA)H^+$ and $(CHCA)_2H^+$, respectively. This result indicates that the ejection of $(CHCA)_2H^+$ ion packet into a vacuum occurs approximately 20 ns behind that observed in $(CHCA)H^+$ packet ejection. However, it is difficult to judge based on the current data whether the magnitude of the electric field affects the ejection time. Still, it can be said that the electric field does not significantly affect t_E. This result is consistent with the ion formation mechanism proceeding in dense gas and clusters at near the sample surface where collisions dominate.[10,13–24]

Based on an analysis of Fig. 6, we obtained the following two new observations. (1) The magnitude of the electric field exhibited little effect on the ejection time, indicating that ion ejection was a thermal process and that the released species reflected the composition of the heated condensed phase and/or near the surface of the MALDI target, and (2) it seems that $(CHCA)_2H^+$ was sequentially produced after the formation of $(CHCA)H^+$, suggesting that the proton transfer reaction of $(CHCA)H^+ + (CHCA)_2 \rightarrow CHCA + (CHCA)_2H^+$ represented the main formation process.

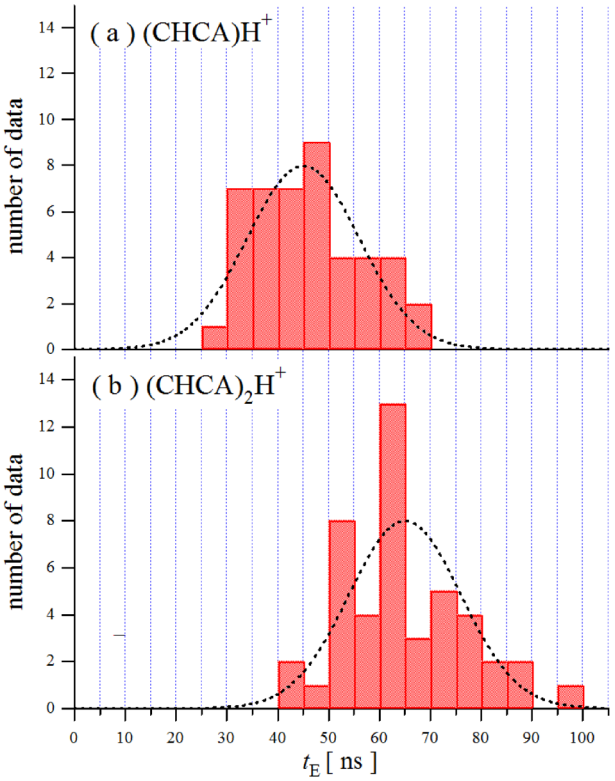

Fig. 6. Distribution of t_E for (a) $CHCAH^+$ and (b) $(CHCA)_2H^+$ obtained from each data in Fig. 5.

CONCLUSION

We developed a method that can trace the ejected and accelerated MALDI ion packets with a temporal resolution of 10 ns using sheet-like UV laser light. The centers of the packets of $(CHCA)H^+$ and $(CHCA)_2H^+$ were observed to eject 46±11 and 64±12 ns after MALDI laser irradiation, respectively. These emission times were not significantly affected by the magnitude of electric field for acceleration, indicating that the emission of ionic species was mainly a thermal process. The delayed ejection of the $(CHCA)_2H^+$ ion packet by approximately 20 ns from the $(CHCA)H^+$ ion packet ejection suggested that $(CHCA)_2H^+$ was formed based on a proton transfer reaction from $(CHCA)H^+$ to $(CHCA)_2$ before vaporization.

The present experimental approach can be applied to various protonated analytes, ions, and neutral species by choosing the laser wavelength, pulse duration, and intensity of LASER-2. Further, we intend to contribute for further understanding the photophysical processes in the MALDI phenomena using this experimental scheme.

Acknowledgements

The authors would like to thank N. Ohta, K. Yokoyama, S. Yokozawa, C. Kawashima, T. Moriyama, and K. Kanazuka for their technical assistance with the experiments. The work was supported by JSPS KAKENHI Grant Numbers JP26410025 and JP18K14889.

REFERENCES

1) M. Karas, F. Hillenkamp. Laser desorption ionization of proteins with molecular masses exceeding 10,000 daltons. *Anal. Chem.* 60: 2299–2301, 1988.
2) M. Karas, D. Bachmann, U. Bahr, F. Hillenkamp. Matrix-assisted ultraviolet laser desorption of non-volatile compounds. *Int. J. Mass Spectrom. Ion Process.* 78: 53–68, 1987.
3) K. Dreisewerd. Recent methodological advances in MALDI mass spectrometry. *Anal. Bioanal. Chem.* 406: 2261–2278, 2014.
4) R. Zenobi, R. Knochenmuss. Ion formation in MALDI mass spectrometry. *Mass Spectrom. Rev.* 17: 337–366, 1998.
5) R. Knochenmuss. Ion formation mechanisms in UV-MALDI. *Analyst* (Lond.) 131: 966–986, 2006.
6) K. Y. Chu, S. Lee, M. T. Tsai, I. -C. Lu, Y. A. Dyakov, Y. H. Lai, Y. T. Lee, C. K. Ni. Thermal proton transfer reactions in ultraviolet matrix-assisted laser desorption/ionization. *J. Am. Soc. Mass Spectrom.* 25: 310–318, 2014. Erratum. *J. Am. Soc. Mass Spectrom.* 25: 1087, 2014.
7) S. H. Ahn, K. M. Park, Y. J. Bae, M. S. Kim. Quantitative reproducibility of mass spectra in matrix-assisted laser desorption ionization and unraveling of the mechanism for gas-phase peptide ion formation. *J. Mass Spectrom.* 48: 299–305, 2013.
8) M. Tsuge, K. Hoshina. Investigation of protonation efficiency for amino acids in matrix-assisted laser desorption/ionization. *Bull. Chem. Soc. Jpn.* 83: 1188–1192, 2010.
9) T. Shirota, M. Tsuge, Y. Hikosaka, K. Soejima, K. Hoshina. Detection of neutral species in the MALDI plume using femtosecond laser ionization: Quantitative analysis of MALDI-MS signals based on a semiequilibrium proton transfer model. *J. Phys. Chem. A* 121: 31–39, 2017.
10) L. V. Zhigilei, E. Leveugle, B. J. Garrison, Y. G. Yingling, M. I. Zeifman. Computer simulations of laser ablation of molecular substrates. *Chem. Rev.* 103: 321–348, 2003.
11) K. Dreisewerd. The desorption process in MALDI. *Chem. Rev.* 103: 395–426, 2003.
12) M. Karas, R. Kruger. Ion formation in MALDI: The cluster ionization mechanism. *Chem. Rev.* 103: 427–440, 2003.
13) G. R. Kinsel, M. E. Gimon-Kinsel, K. J. Gillig, D. H. Russell. Investigation of the dynamics of matrix-assisted laser desorption/ionization ion formation using an electrostatic analyzer/time-of-flight mass spectrometer. *J. Mass Spectrom.* 34: 684–690, 1999.
14) I. Fournier, A. Brunot, J. C. Tabet, G. Bolbach. Delayed extraction experiments using a repulsive potential before ion extraction: Evidence of clusters as ion precursors in UV-MALDI. Part I: Dynamical effects with the matrix 2,5-dihydroxybenzoic acid. *Int. J. Mass Spectrom.* 213: 203–215, 2002.
15) I. Fournier, A. Brunot, J. C. Tabet, G. Bolbach. Delayed extraction experiments using a repulsing potential before ion extraction: Evidence of non-covalent clusters as ion precursor in UV matrix-assisted laser desorption/ionization. Part II: Dynamic effects with α-cyano-4-hydroxycinnamic acid matrix. *J. Mass Spectrom.* 40: 50–59, 2005.
16) E. Sachon, G. Clodic, T. Blasco, G. Bolbach. Protein desolvation in UV matrix-assisted laser desorption/ionization (MALDI). *J. Am. Soc. Mass Spectrom.* 18: 1880–1890, 2007.
17) M. Karas, M. Glückmann, J. Schäfer. Ionization in matrix-assisted laser desorption/ionization: Singly charged molecular ions are the lucky survivors. *J. Mass Spectrom.* 35: 1–12, 2000.
18) T. W. Jaskolla, M. Karas. Compelling evidence for lucky survivor and gas phase protonation: The unified MALDI analyte protonation mechanism. *J. Am. Soc. Mass Spectrom.* 22: 976–988, 2011.
19) L. Diologent, G. Bolbach, C. Focsa, M. Ziskind, I. Fournier. Laser induced post-desolvation of MALDI clusters. *Int. J. Mass Spectrom.* 416: 29–36, 2017.
20) L. V. Zhigilei. Dynamics of the plume formation and parameters of the ejected clusters in short-pulse laser ablation. *Appl. Phys., A Mater. Sci. Process.* 76: 339–350, 2003.
21) L. V. Zhigilei, P. B. S. Kodali, B. J. Garrison. Molecular dynamics model for laser ablation and desorption of organic solids. *J. Phys.*

Chem. B 101: 2028–2037, 1997.

22) L. V. Zhigilei, Y. G. Yingling, T. E. Itina, T. A. Schoolcraft, B. J. Garrison. Molecular dynamics simulations of matrix-assisted laser desorption-connections to experiment. *Int. J. Mass Spectrom.* 226: 85–106, 2003.
23) L. V. Zhigilei, B. J. Garrison. Microscopic mechanisms of laser ablation of organic solids in the thermal and stress confinement irradiation regimes. *J. Appl. Phys.* 88: 1281–1298, 2000.
24) R. Knochenmuss, L. V. Zhigilei. Molecular dynamics model of ultraviolet matrix-assisted laser desorption/ionization including ionization processes. *J. Phys. Chem. B* 109: 22947–22957, 2005.
25) R. Knochenmuss. A quantitative model of ultraviolet matrix-assisted laser desorption/ionization. *J. Mass Spectrom.* 37: 867–877, 2002.
26) A. Rohlfing, A. Leisner, F. Hillenkamp, K. Dreisewerd. Investigation of the desorption process in UV matrix-assisted laser desorption/ionization with a liquid 3-nitrobenzyl alcohol matrix by photoacoustic analysis, fast-flash imaging, and UV-laser postionization. *J. Phys. Chem. C* 114: 5367–5381, 2010.
27) A. Leisner, A. Rohlfing, U. Rohling, K. Dreisewerd, F. Hillenkamp. Time-resolved imaging of the plume dynamics in infrared matrix-assisted laser desorption/ionization with a glycerol matrix. *J. Phys. Chem. B* 109: 11661–11666, 2005.
28) A. A. Puretzky, D. B. Geohegan. Gas-phase diagnostics and LIF-imaging of 3-hydroxypicolinic acid MALDI-matrix plumes. *Chem. Phys. Lett.* 286: 425–432, 1998.
29) A. A. Puretzky, D. B. Geohegan, G. B. Hurst, M. V. Buchanan, B. S. Luk'yanchuk. Imaging of vapor plumes produced by matrix assisted laser desorption: A plume sharpening effect. *Phys. Rev. Lett.* 83: 444–447, 1999.
30) V. Bökelmann, B. Spengler, R. Kaufmann. Dynamical parameters of ion ejection and ion formation in matrix-assisted laser desorption/ionization. *Eur. J. Mass Spectrom. (Chichester, Eng.)* 1: 81–93, 1995.
31) M. Karas, U. Bahr, U. Gießmann. Matrix-assisted laser desorption ionization mass spectrometry. *Mass Spectrom. Rev.* 10: 335–357, 1991.
32) P. Juhasz, M. L. Vestal, S. A. Martin. On the initial velocity of ions generated by matrix-assisted laser desorption ionization and its effect on the calibration of delayed extraction time-of-flight mass spectra. *J. Am. Soc. Mass Spectrom.* 8: 209–217, 1997.
33) R. Knochenmuss, L. V. Zhigilei. Molecular dynamics simulations of MALDI: Laser fluence and pulse width dependence of plume characteristics and consequences for matrix and analyte ionization. *J. Mass Spectrom.* 45: 333–346, 2010.